36.0 MICROSTRUCTURAL EVOLUTION IN TITANIUM ALLOYS UNDER ADDITIVE MANUFACTURING CONDITIONS

Alec Saville (Mines)
Faculty: Amy Clarke (Mines)
Other Participants: Jonah Klemm-Toole, Jeremy Shin, and Brian Rodgers (Mines)
Industrial Mentor: Adam Pilchak (AFRL), Collin Donohoue (SNL)

This project initiated in Fall 2018 and is supported by the Office of Naval Research, the Center for Advanvced Non-Ferrous Structural Alloys, and the National Science Foundation. The research performed during this project will serve as part of the basis for a Ph.D. thesis program for Alec Saville.

36.1 Project Overview and Industrial Relevance

Over the last decade, metallic additive manufacturing (AM) has seen increasing use in the creation of near-net shape functional and low-risk structural components. The primary benefit of AM over traditional manufacturing processes is the ability to create custom geometries beyond what is possible with traditional manufacturing processes, and to reduce the waste associated with extensive machining [36.1-4]. One of the main challenges of AM is maintaining control of material properties and microstructure via careful selection of build parameters. Porosity, cracking, anisotropic loading response, and unintended microstructural characteristics are all possible defects in AM builds, potentially leading to metallic AM being restricted to low-risk applications [36.5-8]. The influence of processing parameters such as scan strategy and layer thickness on material performance, microstructural evolution, and defect formation are not well understood and are an active area of materials research.

This project focuses on analyzing additively manufactured Ti-6Al-4V produced via an AM electron beam melted (EBM) powder process to evaluate the influence of processing conditions on crystallographic texture and anisotropic loading responses. Three specimens of EBM Ti-6Al-4V were produced at Oak Ridge National Laboratory (ORNL) with different scan strategies identified as Raster, Dehoff, and Random. Random and Dehoff are spot-based methods, deposting material in spots instead of in a linear fashion (**Figure 36.1**). Raster is a traditional deposition process, where material is deposited linearly every layer and the travel path rotated 67.5° between layers (**Figure 36.2**).

These scan strategies alter the local thermal history of each build and give rise to potentially different crystallographic texture (known from here in shorthand as texture). Differences in texture are important to controlling anisotropic behavior in AM builds. By quantifying these differences, this work aims to develop a greater understanding of how anisotropic behavior evolves for additively manufactured metallic alloys. Texture can also be a diagnostic tool to monitor phase transformations or other microstructural phenomenon, and can provide additional insight into how a material responds to different AM build conditions.

36.2 Previous Work

36.2.1 Literature Review of Additive Manufacturing of Ti-6Al-4V

A survey of additive manufacturing literature pertaining to Ti-6Al-4V and EBM build processes was completed to give a general background for future work. EBM Ti-6Al-4V differs microstructurally from laser based powder bed build (LBPF) processes, due to decreased cooling rates as a result of the heated build chambers intrinsic to this variant of AM. EBM builds exhibit colony $\alpha + \beta$ microstructures with potential Widmansttatten α or martensitic α', depending on build chamber temperature and build parameters [36.4, 36.9-11], while laser builds exhibit an almost completely martensitic microstructure. This latter microstructure forms due to the lack of a heated chamber in LPBF builds, resulting in an increased cooling rate and thus a microstructure dominated by α' [36.12-16].

It is worth noting EBM builds are thought to exhibit an α' microstructure directly after the initial deposition of a layer of material. This decomposes into fine $\alpha + \beta$ lamellae during subsequent layer depositions due to higher ambient temperature, and has been shown to increase both ductility and strength of Ti-6Al-4V [36.5]. LPBF builds can achieve similar microstructures through careful manipulation of build parameters, but the process is more involved than typically seen in EBM. [36.17-18]

Crystallographic texture for AM Ti-6Al-4V is normally weak (1.5-2 multiples of random distribution). Immediately after deposition, a strong cubic solidification {001} fiber texture is exhibited by the β-Ti phase. After cooling below the β-transus temperature, most β-Ti transforms into α-Ti with relatively weak texture. With the next deposition pass, the newly deposited material solidifies as β-Ti and grows epitaxially on previously deposited layers heated into the β-regime. This process effectively cycles the previous few layers of a Ti-6Al-4V build through a repeated $\beta \leftrightarrow \alpha$ transformation, washing out any major α-Ti texture which may appear [36.5, 36.19-20]. Thus, it is expected to find relatively weak α-Ti texture in this work.

36.2.2 Neutron Diffraction Experiments and Training on Processing Neutron Diffraction Data

Neutron diffraction data was collected in Q3-2018 at Los Alamos National Laboratory (LANL) for the Random, Raster, and Dehoff specimens. Both bulk and local diffraction experiments were completed (**Figure 36.2**) to collect crystallographic texture information between specimens and as a function of build height. In Q4-2018 to Q2-2019, training on processing neutron diffraction data using the Material Analysis Using Diffraction (MAUD) software package was also completed with the guidance of LANL scientists. These activities laid the groundwork for the recent progress reported below.

36.2.3 Processing of Neutron Diffraction Data

Using an iterative approeach with the MAUD software package, a consistent and stable operating route was developed to process neutron diffraction data. Specific values including lattice parameters derived from X-ray diffraction (XRD) and the Debye-Waller thermal attenuation factor from past studies were required and found with additional investigations. All experimental datasets obtained from LANL were run through the updated processing route, and the results were exported into the MATLAB-MTEX plugin for quantification. Both α-Ti and β-Ti texture information were generated, but only α-Ti information is reported here. This is due to a relatively low phase fraction of β-Ti from each specimen (below the required 5 vol % value for sufficient neutron diffraction signal), reducing the confidence in any calculated results.

The MATLAB-MTEX plugin generates recalculated pole figures (**Figure 36.3)** and orientation distribution functions (ODF) (**Figure 36.4**), giving semi-quantitative and quanitative texture information, respectively. Preferred orientations for each diffraction experiment (from here on referred to as texture components) were extracted from ODF's and relative volume fractions of each texture component evaluated. Such a calculation allows for a quantitative comparison between each experiment by observing changes in component volume fraction as a function of scan strategy and build height. This avoids semi-quantiative interpretations of texture information associated with pole figures and can also illustrate any fiber textures present within the material.

Initial processing indicated a suspected basal fiber texture present in all three specimens, as seen in **Figure 36.5**, which was thought to be evidence of the Burger's orientation relationship between α-Ti and β-Ti, assuming a strong (001) β-Ti solidification texture.

36.3 Recent Work

36.3.1 Crystallographic Texture Review of Titanium Alloys

In order to provide context for the results collected from ODF's, a second literature review was completed for Ti-6Al-4V and similar systems. The primary objective of this search was to identify previously reported texture components in both AM and traditional processing studies and to compare these values to those found in this work. In many material systems, specific texture components indicate distinct microstructural evolution phenomena and give insight into material changes during processing (*e.g.* recrystallization). Such insight would assist in controlling the microstructure of metallic AM builds, bringing AM one step closer to creating born-qualified components.

Updated comparisons of texture components found in literature to those observed in MTEX demonstrated noticeable differences, with minimal to no overlap for all experiments. Other studies with EBM Ti-6Al-4V have produced similar textures to those seen in **Figure 36.4,** but did not perform any quantification of individual components. Further investigation determined most studies (both AM and traditional manufacturing) imply what is known as an orthotropic specimen symmetry in their texture analysis, assuming a statistical symmetry due to processing of the material (*e.g.*

rolling). Such an assumption is supported by the presence of an apparent symmetry in pole figures and texture components, which repeat at constant intverals throughout an ODF.

Such symmetry and periodicity is not observed in **Figure 36.4** or **Figure 36.5** however, and indicates a triclinic specimen symmetry is more applicable for all three specimens. Such a triclinic assumption has been enforced in the processing of texture data here after consulting with Adam Pilchak (AFRL) and Adam Creuziger (NIST). It is also the author's recommendation that other studies of crystallographic texture in additive manufacturing enact the same assumption to capture all possible texture components of a given build process.

It was also discovered that no standard reference frame for reporting texture in additive manufacturing has been developed, making comparisons with other texture studies prohibitive. It is the additional recommendation of the author to standardize a specimen reference frame as seen in **Figure 36.6** to enable consistent reporting of texture components and to improve the development of crystallographic texture as a diagnostic tool for additive manufacturing.

36.3.2 Quantification of Texture Components

Parallel to the updated literature review of crystallographic texture components, quantification of each primary texture component was completed for all bulk and local neutron diffraction experiments. The top six texture components from each ODF were selected for analysis, and the volume fractions of each component were calculated. All other texture components were assumed to contribute little to the overall crystallopgrahic texture, with intensities at or below 2 multiples of random distribution (mrd). An example quantification can be observed in **Figure 36.7.**

As mentioned in section **36.3.1**, effectively all reported texture components deviated from literature values, due to the assumption of an orthotropic specimen symmetry in the literature. Thus, no similar quantification has been completed to date and this work represents the first known triclinic specimen symmetry study of AM titanium reported at the time of writing.

It was found during quantification that common texture components were observed between scan strategies and throughout the build height of two or more specimens. This finding was unexpected, given the largely different thermal histories for each specimen. **Figure 36.8** lists these components in greater detail, and shows which components are common to which scan strategies. Physical interpretation of the component has yet to be completed, but is part of the present focus for this work. Section **36.3.3** below provides more information on how this will be accomplished.

36.3.3 Large Scale Electron Back Scatter Diffraction

To develop context for each quantified texture component, large scale electron backscatter diffraction (EBSD) maps of each specimen were collected with the help of Jake Benzing at NIST-Boulder. These studies analyzed the surface as seen in **Figure 36.9,** and evaluated 4 mm x 4 mm regions up the build height of each specimen. An example map tracking only α-Ti orientations can be observed in **Figure 36.10.**

Using a 1 micron step size, these large scale maps were collected to accomplish multiple objectives. With such a large area of analysis, these EBSD maps can produce statistically significant crystallographic texture information to compare with prior neutron diffraction findings. This gives insight into how representative neutron diffraction is of local crystallographic texture, and illustrates any need for revisions on how the raw neutron diffraction data was processed in MAUD.

A qualitative comparison of both EBSD and neutron diffraction data for the map illustrated in **Figure 36.10** is shown in **Figure 36.11**. The similar profile of preferred orientations and intensities demonstrated by the neutron diffraction and EBSD data shows both techniques reported the same overall preferred orientations, validating the MAUD processing completed at the beginning of this project and showing neutron diffraction can screen texture as a function of build height. These findings also enable the completion of the two following additional experimental objectives.

The secondary goal of collecting large scale EBSD maps is to develop a direct microstructural link for each texture component reported in neutron diffraction. Each mapped grain corresponds to a specific texture component consisting of a series of Euler angles, but also corresponds to a certain grain size, morphology, and spatial location. This information can be used to isolate the primary texture components intrinsic to each neutron diffraction experiment within the actual microstructure, and relates these to actual grains within an AM build on the basis of morphology and microstructural evolution. Such a correlation can be completed for any texture component, and will be done for all primary and common texture components reported from neutron diffraction. This is an incredibly powerful correlation, enabling previously unknown crystallographic texture-microstructure relationships to be used for control of anisotropy and microstructure in AM parts. At this time, this phase of work is still in its infancy, but is the primary focus of future endeavors.

These EBSD maps also enable a third objective to be completed. As previously reported, neutron diffraction could not probe texture for β-Ti due to a reduced secondary phase fraction. Such information is critical for understanding the full texture evolution of AM titanium alloys, given the material first solidifies as β-Ti and then transforms into the α-Ti phase. These large scale orientation maps allow for the backcalcluation of the β-Ti texture and can be used to gain further insight into how scan strategy and build height alters preferred orientations in AM materials. Such recalculations will be completed in Q2-2020 with the help of Adam Pilchak (AFRL).

36.4 Plans for Next Reporting Period

Future work will focus on completing smaller scale EBSD maps to quantify phase fractions for each scan strategy employed here, publishing a summary of ongoing texture work, developing/publishing a standard operating procedure for processing neutron diffraction data, and transitioning to new studies on the development of Ti alloys for additive manufacturing.

- Complete small scale EBSD maps for phase quantification;
- Publish texture component paper in Q1 or Q2-2020;
- Develop instructional and explanatory documentation (video tutorials and documents) for using MAUD software package;
- Begin literature review for Ti alloy systems designed for additive manufacturing;

36.5 References

[36.1] Dutta, B., Froes, F.H. (Sam), 2017. The Additive Manufacturing (AM) of titanium alloys. Metal Powder Report 72, 96–106. https://doi.org/10.1016/j.mprp.2016.12.062

[36.2] Frazier, W.E., 2014. Metal Additive Manufacturing: A Review. Journal of Materials Engineering and Performance 23, 1917–1928. https://doi.org/10.1007/s11665-014-0958-z

[36.3] Liu, S., Shin, Y.C., 2019. Additive manufacturing of Ti6Al4V alloy: A review. Materials & Design 164, 107552. https://doi.org/10.1016/j.matdes.2018.107552

[36.4] Sames, W.J., List, F.A., Pannala, S., Dehoff, R.R., Babu, S.S., 2016. The metallurgy and processing science of metal additive manufacturing. International Materials Reviews 61, 315–360. https://doi.org/10.1080/09506608.2015.1116649

[36.5] Al-Bermani, S.S., Blackmore, M.L., Zhang, W., Todd, I., 2010. The Origin of Microstructural Diversity, Texture, and Mechanical Properties in Electron Beam Melted Ti-6Al-4V. Metallurgical and Materials Transactions A 41, 3422–3434. https://doi.org/10.1007/s11661-010-0397-x

[36.6] Brice, C.A., Tayon, W.A., Pilchak, A.L., 2014. Texture Development in Titanium Components Made by Additive Manufacturing. San Diego 16.

[36.7] Butler, T.M., Brice, C.A., Tayon, W.A., Semiatin, S.L., Pilchak, A.L., 2017. Evolution of Texture from a Single Crystal Ti-6Al-4V Substrate During Electron Beam Directed Energy Deposition. Metallurgical and Materials Transactions A 48, 4441–4446. https://doi.org/10.1007/s11661-017-4219-2

[36.8] Chandramohan, P., 2019. Laser additive manufactured Ti-6Al-4V alloy: Texture analysis. Materials Chemistry and Physics 226, 272–278. https://doi.org/10.1016/j.matchemphys.2019.01.035

[36.9] Körner, C., 2016. Additive manufacturing of metallic components by selective electron beam melting — a review. International Materials Reviews 61, 361–377. https://doi.org/10.1080/09506608.2016.1176289

[36.10] Murr, L.E., 2015. Metallurgy of additive manufacturing: Examples from electron beam melting. Additive Manufacturing 5, 40–53. https://doi.org/10.1016/j.addma.2014.12.002

[36.11] Tan, X., Kok, Y., Toh, W.Q., Tan, Y.J., Descoins, M., Mangelinck, D., Tor, S.B., Leong, K.F., Chua, C.K., 2016. Revealing martensitic transformation and α/β interface evolution in electron beam melting three-dimensional-printed Ti-6Al-4V. Scientific Reports 6. https://doi.org/10.1038/srep26039

[36.12] Chastand, V., Tezenas, A., Cadoret, Y., Quaegebeur, P., Maia, W., Charkaluk, E., 2016. Fatigue characterization of Titanium Ti-6Al-4V samples produced by Additive Manufacturing. Procedia Structural Integrity 2, 3168–3176. https://doi.org/10.1016/j.prostr.2016.06.395

[36.13] Juechter, V., Scharowsky, T., Singer, R.F., Körner, C., 2014. Processing window and evaporation phenomena for Ti–6Al–4V produced by selective electron beam melting. Acta Materialia 76, 252–258. https://doi.org/10.1016/j.actamat.2014.05.037

[36.14] Kobryn, P.A., Semiatin, S.L., 2001. The laser additive manufacture of Ti-6Al-4V. JOM 53, 40–42. https://doi.org/10.1007/s11837-001-0068-x

[36.15] Nandwana, P., Lee, Y., Ranger, C., Rollett, A.D., Dehoff, R.R., Babu, S.S., 2019. Post-processing to Modify the α Phase Micro-Texture and β Phase Grain Morphology in Ti-6Al-4V Fabricated by Powder Bed Electron Beam Melting. Metallurgical and Materials Transactions A 50, 3429–3439. https://doi.org/10.1007/s11661-019-05247-4

[36.16] Thijs, L., Verhaeghe, F., Craeghs, T., Humbeeck, J.V., Kruth, J.-P., 2010. A study of the microstructural evolution during selective laser melting of Ti–6Al–4V. Acta Materialia 58, 3303–3312. https://doi.org/10.1016/j.actamat.2010.02.004

[36.17] Xu, W., Brandt, M., Sun, S., Elambasseril, J., Liu, Q., Latham, K., Xia, K., Qian, M., 2015. Additive manufacturing of strong and ductile Ti–6Al–4V by selective laser melting via in situ martensite decomposition. Acta Materialia 85, 74–84. https://doi.org/10.1016/j.actamat.2014.11.028

[36.18] Yang, J., Yu, H., Yin, J., Gao, M., Wang, Z., Zeng, X., 2016. Formation and control of martensite in Ti-6Al-4V alloy produced by selective laser melting. Materials & Design 108, 308–318. https://doi.org/10.1016/j.matdes.2016.06.117

[36.19] Pesach, A., Tiferet, E., Vogel, S.C., Chonin, M., Diskin, A., Zilberman, L., Rivin, O., Yeheskel, O., Caspi, E.N., 2018. Texture analysis of additively manufactured Ti-6Al-4V using neutron diffraction. Additive Manufacturing 23, 394–401. https://doi.org/10.1016/j.addma.2018.08.010

[36.20] Vogel, S.C., Takajo, S., Kumar, M.A., Caspi, E.N., Pesach, A., Tiferet, E., Yeheskel, O., 2018. Ambient and High-Temperature Bulk Characterization of Additively Manufactured Ti-6Al-4V Using Neutron Diffraction. JOM 70, 1714–1722. https://doi.org/10.1007/s11837-018-3038-2

36.6 Figures and Tables

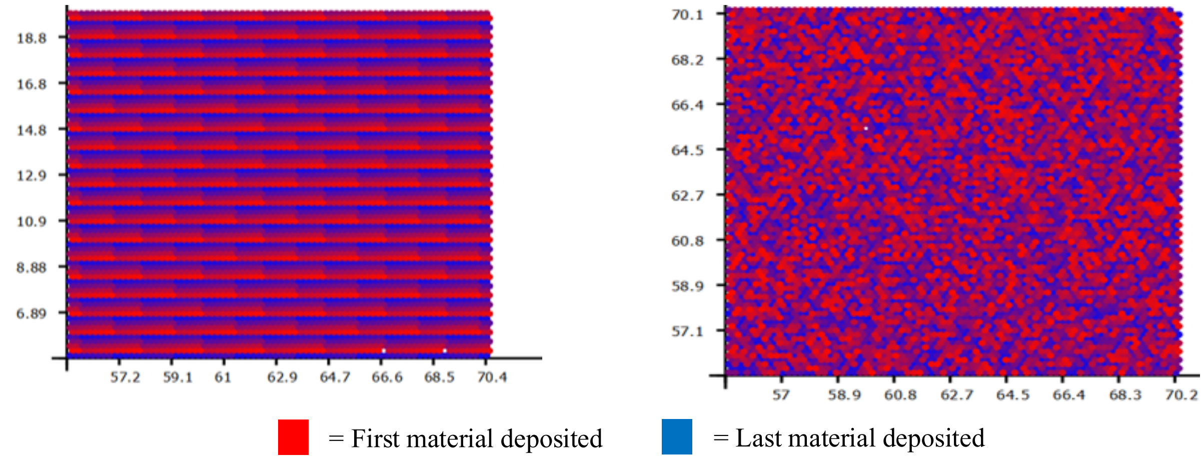

Figure 36.1: Illustrations of the two spot deposition scan strategies Dehoff (left) and Random (right) implemented.

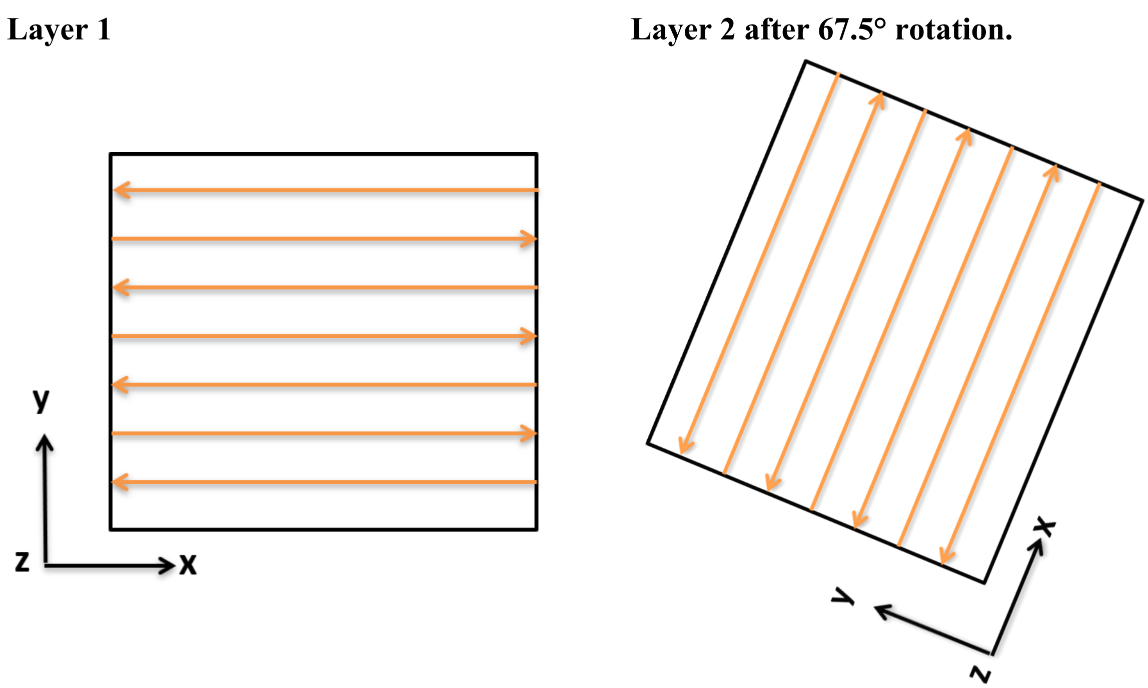

Figure 36.2: Illustration of the Raster scan strategy implemented here. Note the 67.5° rotation between layers incorporated into this build process (right).

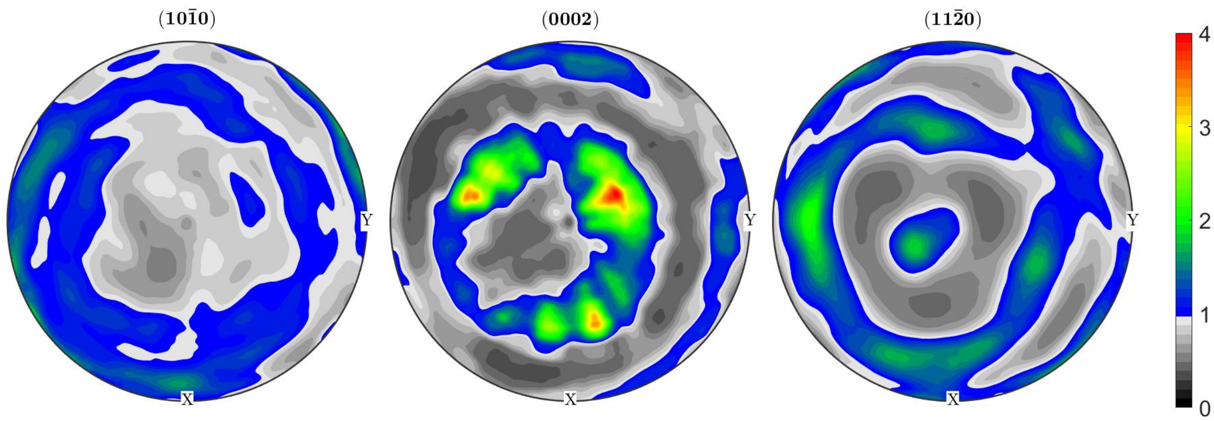

Figure 36.3: Recalculated α-Ti pole figures for a neutron diffraction experiment of the Random scan strategy specimen evaluated 2 mm from the top of the build geometry.

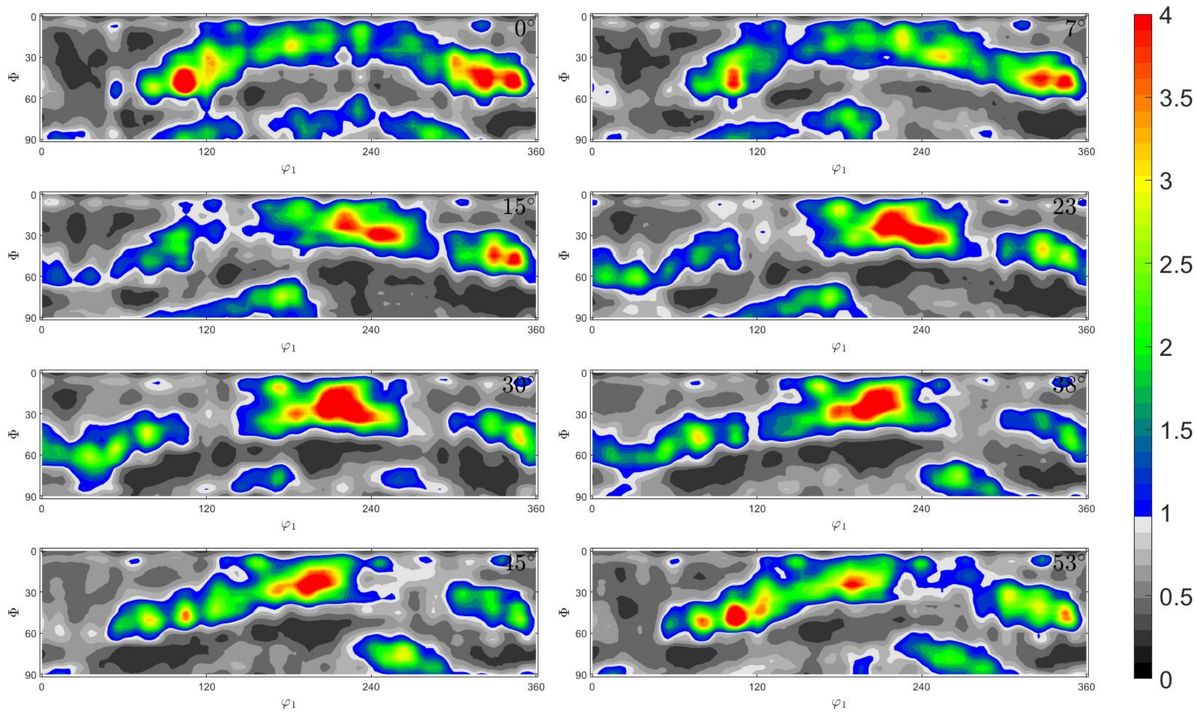

Figure 36.4: Orientation distribution function of the same experiment as **Figure 36.3**. Note the primary texture components (regions of red coloration) present throughout the fiber texture are suspected to be evidence of the Burger's orientation relationship in titanium.

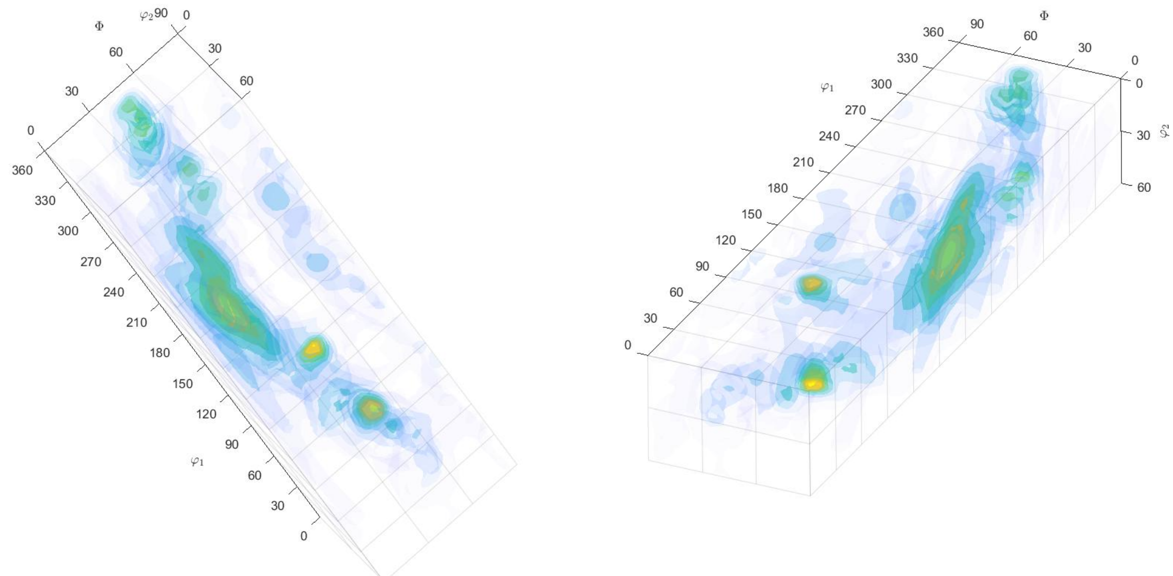

Figure 36.5: 3D ODF illustrating the Random scan strategy fiber texture observed in two-dimensional slices in **Figure 36.4** from assorted angles. Views are selected to help develop perspective on the fiber texture's appearance in 3D.

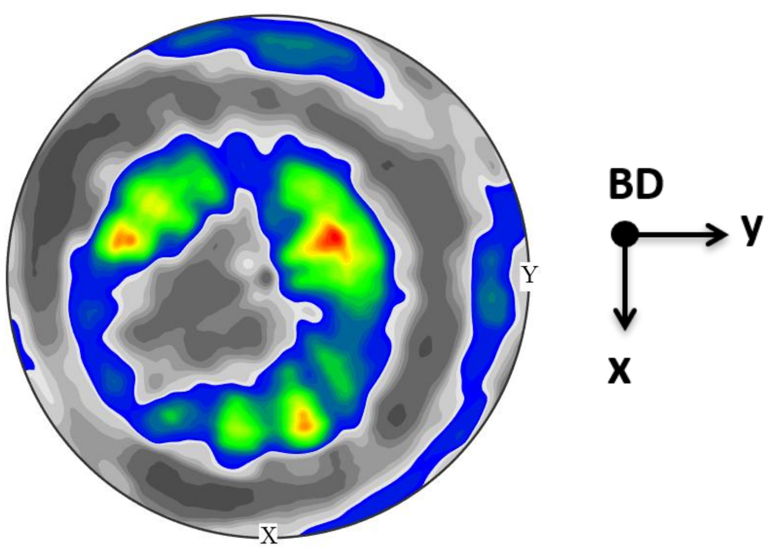

Figure 36.6: Recommended reference frame for studying crystallographic texture in additive manufacturing studies. Note the build direction is out of the the center of the pole figure such that this perspective looks down the build height.

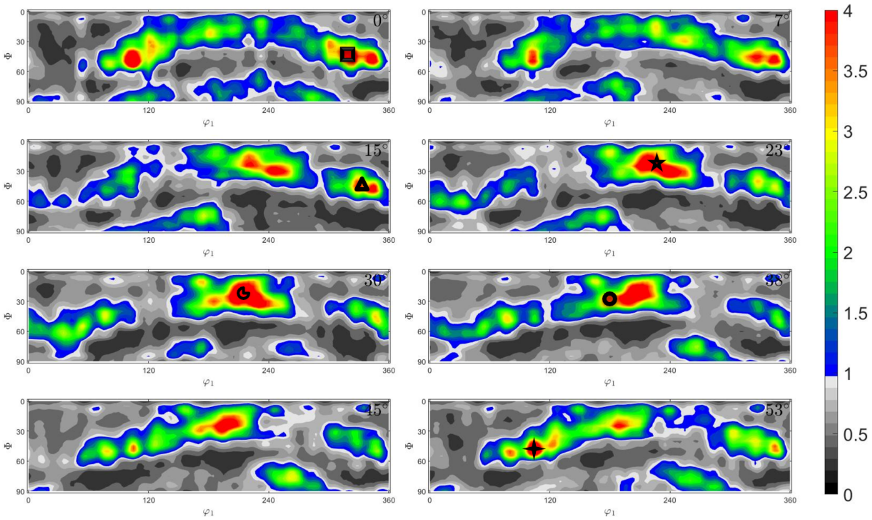

Primary Texture Components

Mark	ϕ_1	Φ	ϕ_2	Volume Fraction (Percent)
✦	104.482	47.1808	54.419	21.247
◔	210.949	26.8216	30.933	21.156
★	237.929	30.9622	22.599	16.284
▲	345.703	48.3243	15.245	15.295
■	324.126	47.1754	3.921	13.901
●	180.640	30.1855	35.009	12.117

Figure 36.7: Example quantification of texture components in the Random scan strategy 2 mm from the build finish. Note the marked regions on the ODF indicating the location of each quantified texture component.

Identifier	Φ_1	Φ	Φ_2
RDL1	208.9	32.1	151.3
RD1	331.4	38.4	13.4
RD2	30.0	59.0	332.8
RL1	55.4	55.5	328.2
DL1	55.8	57.9	297.7
DL2	105.4	45.8	262.7

Key:

R = Found in Random scan strategy
D = Found in Dehoff scan strategy
L = Found in Raster scan strategy

Figure 36.8: Common texture components reported in this work. Note most components were reported only in two scan strategies, while one was reported in all three scan strategies.

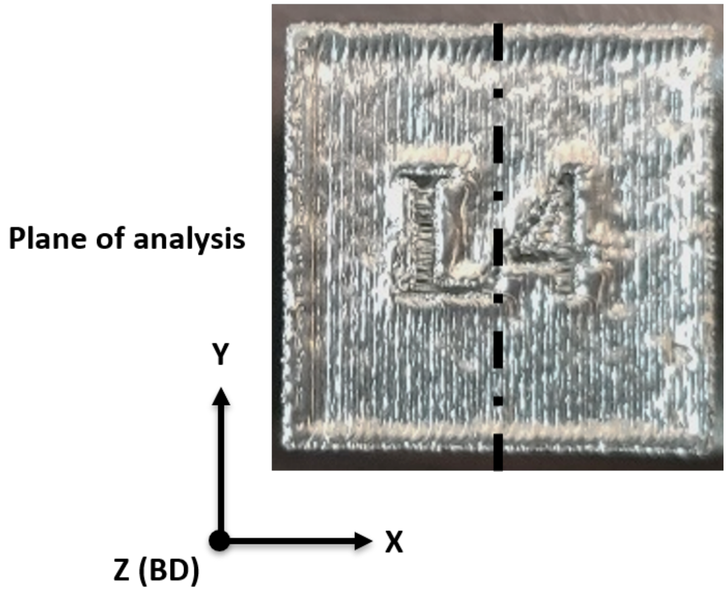

Figure 36.9: Plane of analysis for the large scale EBSD study. Note the build direction oriented out of the page.

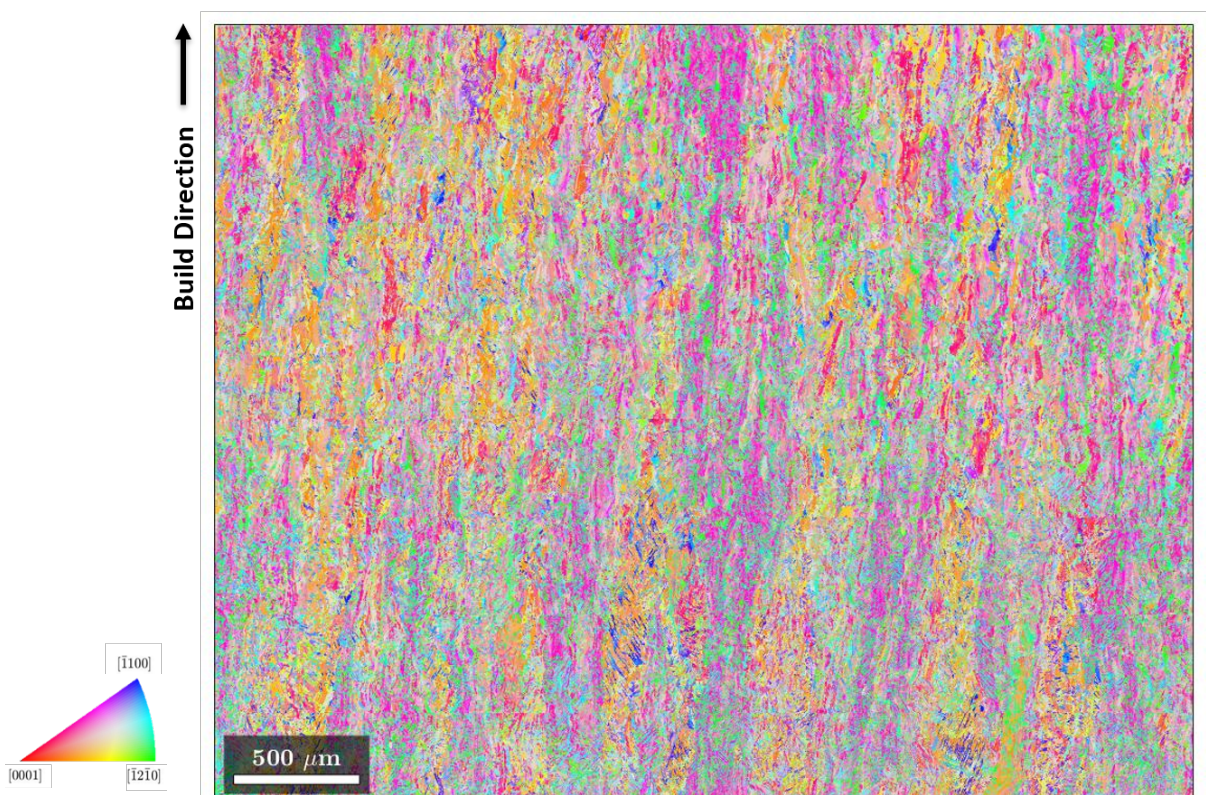

Figure 36.10: Large scale α-Ti EBSD map of the Random scan strategy specimen taken at the first 4 mm of the build height. Note the build direction marked upwards on the page and the periodic regions of pink, orange, and green coloration. The IPF coloration is defined from the y-direction left-right across the image.

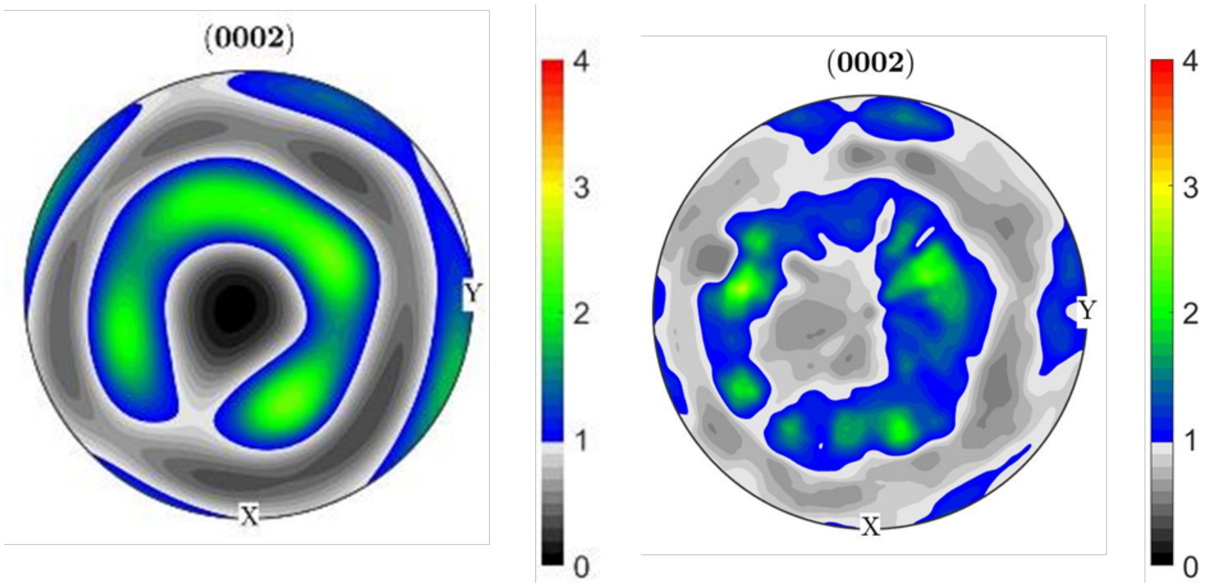

Figure 36.11: α-Ti (0002) pole figures demonstrating similar textures collected from EBSD (left) and neutron diffraction (right) at 3 mm from the build start.